FULL PAPER

Na–Air Batteries

ADVANCED
FUNCTIONAL
MATERIALS

www.afm-journal.de

Visualizing the Oxidation Mechanism and Morphological Evolution of the Cubic-Shaped Superoxide Discharge Product in Na–Air Batteries

Qian Sun, Jian Liu, Biwei Xiao, Biqiong Wang, Mohammad Banis, Hossein Yadegari, Keegan R. Adair, Ruying Li, and Xueliang Sun*

Sodium–air (Na–O$_2$) batteries have recently developed as a high theoretical energy density energy storage and conversion system. In particular, Na–O$_2$ batteries with superoxide as the discharge product have a very high round-trip energy efficiency over lithium–air batteries due to their significantly reduced charging overpotential. However, Na–O$_2$ batteries yet suffer from limited cycling lives because of the formation and incomplete removal of side products during oxygen reduction reaction (ORR) and oxygen evolution reaction (OER) processes, while the mechanism of these processes is still not fully understood. Herein, a detailed investigation on tracking the decomposition pathway of cubic-shaped micrometer-sized NaO$_2$ discharge products in Na–O$_2$ batteries with carbon-based air electrodes is reported. A detailed electrochemical charging mechanism is revealed during the charging process. The evolution of the chemical compositions of the discharge/side products in air electrode during charging is also verified by synchrotron-based X-ray absorption spectroscopy experiments. The formation of these intermediate phases other than NaO$_2$ during the charging process results in high overpotentials. These new findings can contribute to a better understanding and the rational design of future Na–O$_2$ batteries.

1. Introduction

The rapid development of electric vehicles (EVs) and hybrid electric vehicles (HEVs) over the last decade has driven battery researchers to explore new options for power supplies with ultrahigh power and energy densities. State-of-the-art Li-ion batteries (LIBs) are yet insufficient to meet the ever-increasing demands of EVs/HEVs for long-distance or large power output

(acceleration) applications. As a possible alternative, alkali metal–oxygen batteries (i.e., Li–O$_2$,[1] Na–O$_2$,[2] and K–O$_2$[3] batteries) have been receiving increasing attention due to their extraordinarily large theoretical energy densities and gravimetric capacities.

The electrochemical reactions of alkali metal–oxygen batteries can be expressed as the overall equations of 1) $2A^+ + 2e^- + O_2 \leftrightarrow A_2O_2$ and/or 2) $A^+ + e^- + O_2 \leftrightarrow AO_2$ (A = Li, Na, or K), which correspond to the formation of peroxide or superoxide species as discharge products, respectively. Recent studies have reached the understanding that superoxide phases are the initial product of the first-step electrochemical reduction of oxygen gas O$_2$ in these alkali metal–oxygen batteries, even in the cases where the peroxides are the final discharge products.[1c,e,4] The further conversion of superoxide to peroxide can occur through either electrochemical or chemical reactions, which has been widely observed for most Li–O$_2$ batteries, unless the lithium superoxide species can be stabilized by a catalyst.[5] However, many studies on Na–O$_2$ and K–O$_2$ batteries have shown that the corresponding superoxides are found to be relatively stable as the final discharge product. The origin of such differences can be at least partially attributed to the long-known difference between the stability of alkali metal peroxides and superoxides. More recently, new understandings on the oxygen reduction reaction (ORR) and sodium superoxide growth via solution-mediated routes, as opposed to the traditional surface-mediated routes, have been established in Na–oxygen batteries,[6] which are believed to be the predominant mechanism for the formation and growth of NaO$_2$ in Na–O$_2$ batteries.

The formation of micrometer-sized NaO$_2$ cubes in Na–O$_2$ batteries has been widely reported. Confounded by the contradictory experimental observations regarding to the formation and removal of micrometer-sized sodium superoxide and the low electronic conductivity predicted by theoretical calculations, the NaO$_2$ precipitation/dissolution mechanisms via solution-based processes have been proposed for Na–O$_2$ batteries and verified by various groups. The presence of water (and other proton donors) has been revealed to have a profound effect on the electrochemical behavior of Na–O$_2$ batteries.[6] Although

Dr. Q. Sun, Prof. J. Liu, Dr. B. Xiao, Dr. B. Wang, Dr. M. Banis,
Dr. H. Yadegari, K. R. Adair, R. Li, Prof. X. Sun
Department of Mechanical and Materials Engineering
University of Western Ontario
London, Ontario N6A 5B9, Canada
E-mail: xsun@eng.uwo.ca
Prof. J. Liu
School of Engineering
Faculty of Applied Science
University of British Columbia
Kelowna, British Columbia V1V 1V7, Canada

**ADVANCED
SCIENCE NEWS**
www.advancedsciencenews.com

**ADVANCED
FUNCTIONAL
MATERIALS**
www.afm-journal.de

moisture in ambient air is found to be fatal to these batteries due to the promotion of side reactions,[7] Nazar and co-workers discovered that a proper trace amount of water (or proton donor) is highly essential to realizing large discharge capacities and the formation of micrometer-sized cubic NaO_2 as the discharge product.[6] They showed that only a small amount of layer-like discharge product deposit on the surface of the air electrode can be achieved when using the truly dry electrolyte made from a home-made anhydrous salt.[6] Lutz et al. also reported that solution-mediated and surface-mediated ORR of $Na–O_2$ batteries can be altered using different electrolyte solvents.[8] Schröder et al. elucidated the distribution of the discharge product over the cathode in $Na–O_2$ batteries by synchrotron X-ray tomography.[9] Sun et al. reported a conformal film-like NaO_2 as the discharge product on a hierarchical porous carbon spheres air electrode of the $Na–O_2$ battery, which exhibit better reversibility and reduced parasitic side reactions.[10] These fundamental studies have built up the critical understanding of the ORR processes of alkali $Na–O_2$ batteries.

Doubtlessly, unveiling the nature of the charging process of $Na–O_2$ batteries can be equivalently important, especially when taking into consideration the fact that the remaining NaO_2 cubes after prolonged cycles have been observed and believed to be a critical reason for the poor cycling stability of $Na–O_2$ batteries.[11] Nevertheless, the process of NaO_2 removal is still poorly understood. Nazar and co-workers showed that when cubic NaO_2 had been formed as the discharge product in the absence of water (proton donor), a significantly increased charging overpotential was observed,[6] which indicates that it is involved in the activation process of superoxide discharge product decomposition at a low charge overpotential. Very recently, with the help of transmission electron/X-ray microscopy (TEM/STXM), the charging process of discharge product(s) in $Na–O_2$ batteries has been further unveiled. Landa-Medrano et al. carried out an STXM study on fully discharged and partially charged cubic NaO_2.[12] They observed the formation of a core–shell structure with the outer walls being composed of oxygen-containing side products and a sodium superoxide/peroxide core after short charging. The formation of the side product as the result of the reactions between sodium superoxide and solvent has been reported by different groups. Nazar and co-workers reported the existence of sodium carbonate, sodium acetate, and sodium formate in the discharge product of $Na–O_2$ battery using NMR and chemical titration.[13] Our group had also applied in situ X-ray absorption spectroscopy (XAS) mapping and in situ Raman mapping in the study of $Na–O_2$ battery systems.[14] Sun and co-workers[15] and Demortière and co-workers[16] also reported in situ TEM studies on $Na–O_2$ batteries to observe the growth of sub-micrometer-sized NaO_2 cubes ($\approx$400–600 nm) during the discharge process. Sun and co-workers observed a relatively reversible charging process of NaO_2 on a CNT air electrode, during which the NaO_2 cube first underwent a rapid shrinkage in size and only a residential shell remained after full charging.[15] They also observed that the irreversible remnants of NaO_2 + Na_2O_2 mixture accumulated on the electrode surface during cycling. In comparison, Demortière and co-workers[16] observed a similar charging mechanism of NaO_2 on a carbon air electrode similar to that reported by Landa-Medrano et al.. A cubic parasitic shell with a NaO_x-wrapped NaO_2 core was

observed at the beginning of the charging process in a yolk–shell structure. After fully charged, the residual parasitic shells remained. More recently, Peng and co-workers reported an in situ TEM study on a $Na–O_2$ system using CuO nanowires as the air cathode.[17] They observed an irregular shape thin film-like $NaO_2/Na_2O_2/Na_2O$ mixture as the discharge product. The catalytic behavior of the transition metal oxide may have contributed to the $2e^-/4e^-$ ORR process to produce Na_2O_2/Na_2O along with the $1e^-$ ORR toward NaO_2, which explained by follows a similar mechanism as our previous study.[18] Overall, these recent studies have provided important insights into the understanding of the OER process of $Na–O_2$ batteries. Nevertheless, there are still several questions pertaining to the electrochemical decomposition mechanism and morphological/chemical evolution of the large micrometer-sized NaO_2 cubes compared to the reported nanoscale discharge products. Moreover, recent studies had widely reported that NaO_2 is not fully stable in the ether-based electrolytes, causing the decomposition of the electrolytes.[13,19] Therefore, it will also be critical to understand the effect of these side reactions/products on the OER processes of Na–air batteries. Besides, the sodium dendrite growth during the charging process of $Na–O_2$ batteries may cause their interval short circuit, which can be addressed by anode protection.[20]

Herein, we report a detailed investigation and fundamental understanding on the decomposition pathway of cubic shape NaO_2 discharge products of $Na–O_2$ batteries based on two typical carbon air electrodes. The morphological and chemical evolution during the charging process of the cubic discharge products are tracked by scanning electron microscopy (SEM) and energy-dispersive X-ray spectroscopy (EDX) characterizations as well as Raman spectra mapping and synchrotron-based XAS characterizations. Accordingly, we propose a core–shell model to elucidate the removal mechanism of NaO_2 and to clarify the origin of increasing overpotentials during charging of the NaO_2 batteries.

2. Results and Discussion

In the present study, we use polyacrylonitrile (PAN) polymer as the binder for both carbon nanotube (CNT) and N-doped carbon nanotube (NCNT) air electrodes after a survey of the effectiveness of various different binders in our group.[21] The effect of binder in $Li–O_2$ batteries has been emphasized since the study by Nazar and co-workers,[22] which shows possible decomposing of PVDF binder against O_2^-. Recently, Goward and co-workers also reported the instability of PVDF in the presence of NaO_2 in $Na–O_2$ batteries.[23] Compared to our previous study using polyvinylidene difluoride (PVDF) as the binder,[24] the CNT–PAN and NCNT–PAN air electrodes exhibited drastically different electrochemical performance. It is worth noting that previous studies have also found that PAN is unstable in the presence of superoxide/peroxide in a chemical environment.[25] Nevertheless, it is very surprising to reveal here that both CNT–PAN and NCNT–PAN air electrodes exhibit an active electrochemical response in the cyclic voltammetry (CV) testing. For the CNT–PAN air electrode (**Figure 1**a), one cathodic and two anodic current peaks can be identified in
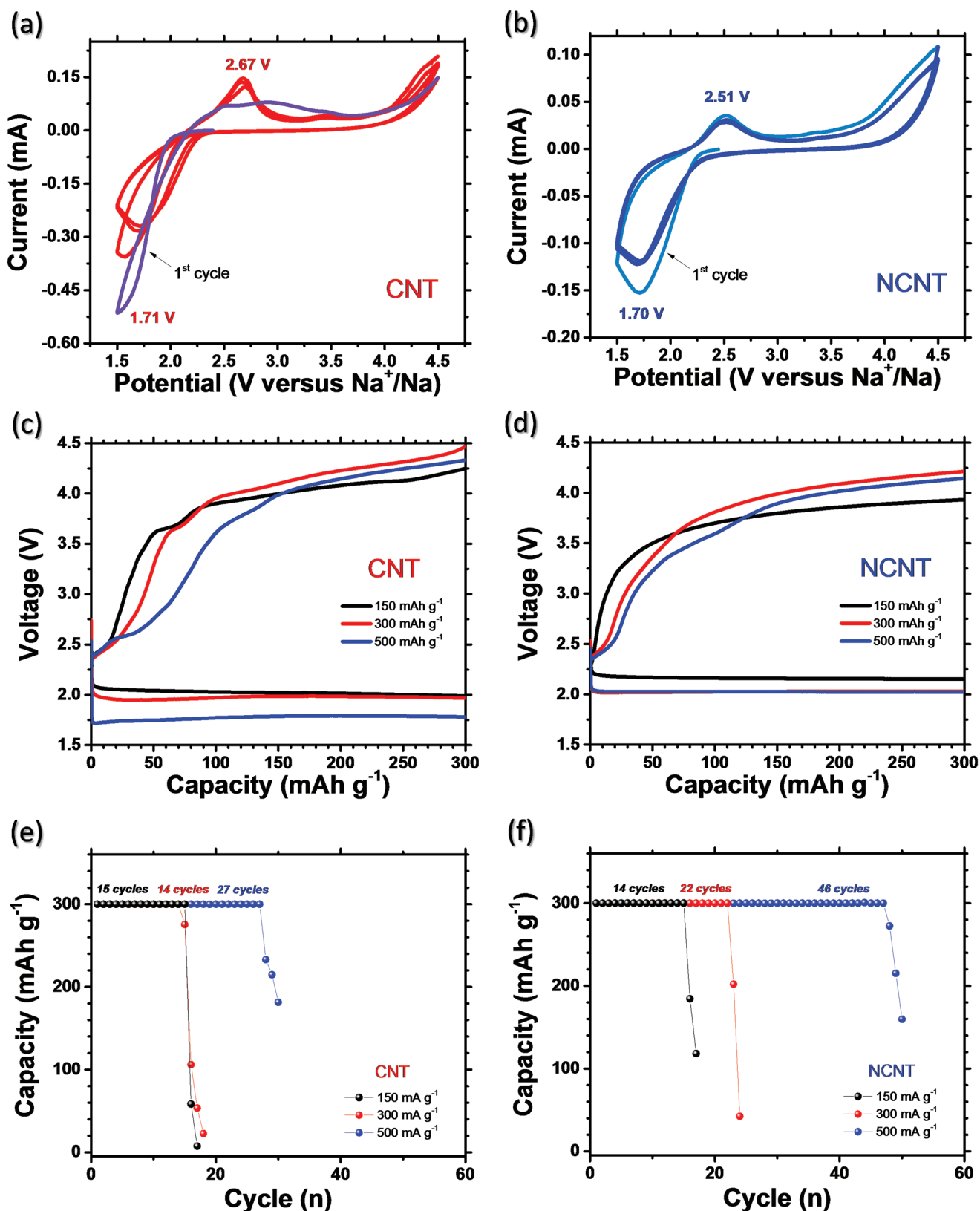
ADVANCED
SCIENCE NEWS
www.advancedsciencenews.com

ADVANCED
FUNCTIONAL
MATERIALS
www.afm-journal.de

Figure 1. CV curves of Na–air batteries with a) CNT–PAN and b) NCNT–PAN air electrode; charge and discharge profiles of SABs with c) CNT–PAN and d) NCNT–PAN air electrodes at the current densities of 150, 300, and 500 mA g^{-1} at the same cutoff capacity of 300 mAh g^{-1}; cycling retention of Na–air batteries with e) CNT–PAN and f) NCNT–PAN air electrodes at different current densities at the same cutoff capacity of 300 mAh g^{-1}.

**ADVANCED
SCIENCE NEWS**

www.advancedsciencenews.com

**ADVANCED
FUNCTIONAL
MATERIALS**

www.afm-journal.de

the first cycle located at around 1.5 V and 2.46/2.91 V, respectively. In the subsequent cycles, only one pair of cathodic and anodic current peaks was observed at 1.71 and 2.67 V, respectively, which can be assigned to the electrochemical reaction of $O_2 + e^- \longleftrightarrow O_2^-$. The 2nd, 3rd, and 4th CV curves overlap well, indicating a highly reversible reaction. The onset of the ORR and OER potentials was found to be 2.32 and 2.20 V, respectively, which are in good agreement with the theoretical thermodynamics potentials of the electrochemical reactions of 1) $2Na^+ + 2e^- + O_2 \leftrightarrow Na_2O_2$ (2.33 V) and/or 2) $Na^+ + e^- + O_2 \leftrightarrow NaO_2$ (2.27 V), respectively.[26] In the case of the NCNT–PAN electrode, the CV curves show further improved reversibility (Figure 1b). In spite of the reduced peak current from the first cycle, all four CV scans exhibited very similar features: a cathodic peak at 1.70 V and two anodic peaks located at 2.51 and 4.3 V. Similarly, to the CNT–PAN electrode, the 2nd to 4th CV curves also indicate excellent reversibility. The onset of the ORR and OER potentials for the NCNT–PAN air electrode was found to be 2.28 and 2.22 V, respectively. It can be concluded that NCNT–PAN air electrode has an improved ORR/OER catalytic performance over the CNT–PAN air electrode, which is consistent with our previous study using PVDF binder.[24]

Moreover, it is revealed that the CNT–PAN and NCNT–PAN air electrodes can be charged and discharged at relatively high current densities up to 500 mA g^{-1} (Figure 1c,d). In contrast, the CNT–PVDF and NCNT–PVDF air electrodes could hardly be discharged and charged in our previous study with the same cell configuration.[26] Meanwhile, the cycling lives of the CNT–PAN and NCNT–PAN air electrodes (Figure 1e,f) are also found to be prolonged compared to those of the CNT–PVDF and NCNT–PVDF air electrodes.[24] When cycled at 500 mA g^{-1} with a cutoff capacity of 300 mAh g^{-1}, the NCNT–PAN air electrodes exhibited a cycling life of 46 cycles before decaying. In addition, the full charge and discharge performances of CNT–PAN and NCNT–PAN electrodes are also compared in Figure S1 (Supporting Information).

We attribute the improved electrochemical performance of the CNT–PAN and NCNT–PAN air electrodes to the effect of the released proton H^+ from the PAN chains, which plays an important role in the electrochemical behavior of the cells. It has been shown by Nazar and co-workers that proton donors are critical in the formation of cubic NaO_2 discharge products in Na–O$_2$ batteries through a solution-mediated route,[6] as also evidenced by electron spin resonance (ESR) spectroscopy.[27] They proved that a trace amount of water (≈10 ppm) in ether electrolyte is essential to achieving acceptable discharge capacities and it can aid in the decomposition of NaO_2 at lower overpotentials.[6] These results differ greatly when an electrolyte containing 0 ppm water is used, resulting in two charging voltage plateaus around 2.7 and 4.2 V in contrast to the single voltage plateau around 2.5 V for the electrolyte containing trace amounts of water. In our recent study on the effect of binders on the practical electrochemical performance of Na–air batteries,[21] we have identified the reaction mechanisms of the binders involved in the electrochemical processes in Na–air batteries and show that the performance is highly dependent on the type of the functional group, i.e., electron-withdrawing group (EWG) and electron-donating group (EDG), in the polymer chain. It is well known that the −CN in the side chain

of PAN is a very strong EDG, which results in the significantly increased acidity of the α-C–H. More mechanism discussions are presented in our study on the survey of various binders for Na–air batteries.[21]

In order to verify the above assumptions, SEM characterizations has been carried out to study the morphology of the discharge product. The SEM images of the CNT–PAN air electrodes in the first cycle at different states of charge and a current density of 500 mA g^{-1} are shown in **Figure 2**a–f. It is clearly observed that massive micrometer-sized cube-shaped discharge products formed after discharging (Figure 2c,d; Figure S2, Supporting Information) which were not present on the initial air electrode (Figure 2a,b). It is consistent with the morphology of sodium superoxide discharge products previously reported.[11] The chemical nature of the discharge product is further confirmed by Raman spectra. The feature at 1056 cm^{-1} as shown in Figure 2l-1 can be attributed to NaO_2.[11] Interestingly, the morphology of the CNT–PAN air electrode after a full charge shows that a unique framework structure remains on the surface of the air electrode (Figure 2i,j; Figure S3, Supporting Information). It is natural to hypothesize that these "frames" after charging should be the remaining undecomposed part of the cubic discharge product, especially considering the similarity between them in terms of both shape and size. The reasoning behind these morphological features and their composition should be identified.

In order to elucidate the origins of the frame-type morphological features, SEM characterization of partially recharged CNT–PAN air electrodes has been carried out and the images are shown in Figure 2e–h. It can be observed that (broken) hollow boxes are found at this charged stage partially 3.5 V. Recently, Landa-Medrano et al. also reported that an ≈300 nm thick outer wall with an oxygen-containing side product (OSP), had separated from the sodium superoxide and peroxide core after short charging (≈17%, to ≈2.45 V), forming a "matryoshka" cube in box structure.[12] Therefore, it can be hypothesized that the remaining outer frame during partial charging in the present study may also compose of carbonate species, which requires higher potentials to be fully decomposed. This assumption is also consistent with the fact that most of these self-standing boxes are removed after fully charged, leaving only framework products.

To further confirm this hypothesis, we carried out a Raman mapping measurement on the partially charged CNT–PAN air electrode (Figure 2k). In contrast to NaO_2 which is detected in the discharged air electrode, no obvious features related to superoxide species were found in the observed region (Figure 2l). However, in addition to the peaks assigned to D and G band of carbon, two new features at 1080 and 1036 cm^{-1} are observed, which can be assigned to Na_2CO_3 and $Na_2O_2\cdot2H_2O$, respectively.[28] The distribution of these two species are then identified by analyzing their corresponding peak intensities and compared to the optical image of the region. From this comparison, it can be concluded that the distribution of the two phases are clearly different. Carbonates appear to distribute at the outer surface, while the hydrated peroxide seems to exist in the inner core. Considering the barely contacting of the carbonate outer shell with the carbon in air cathode, it may be inferred that the major source of Na_2CO_3 in this structure is likely to be attributed to
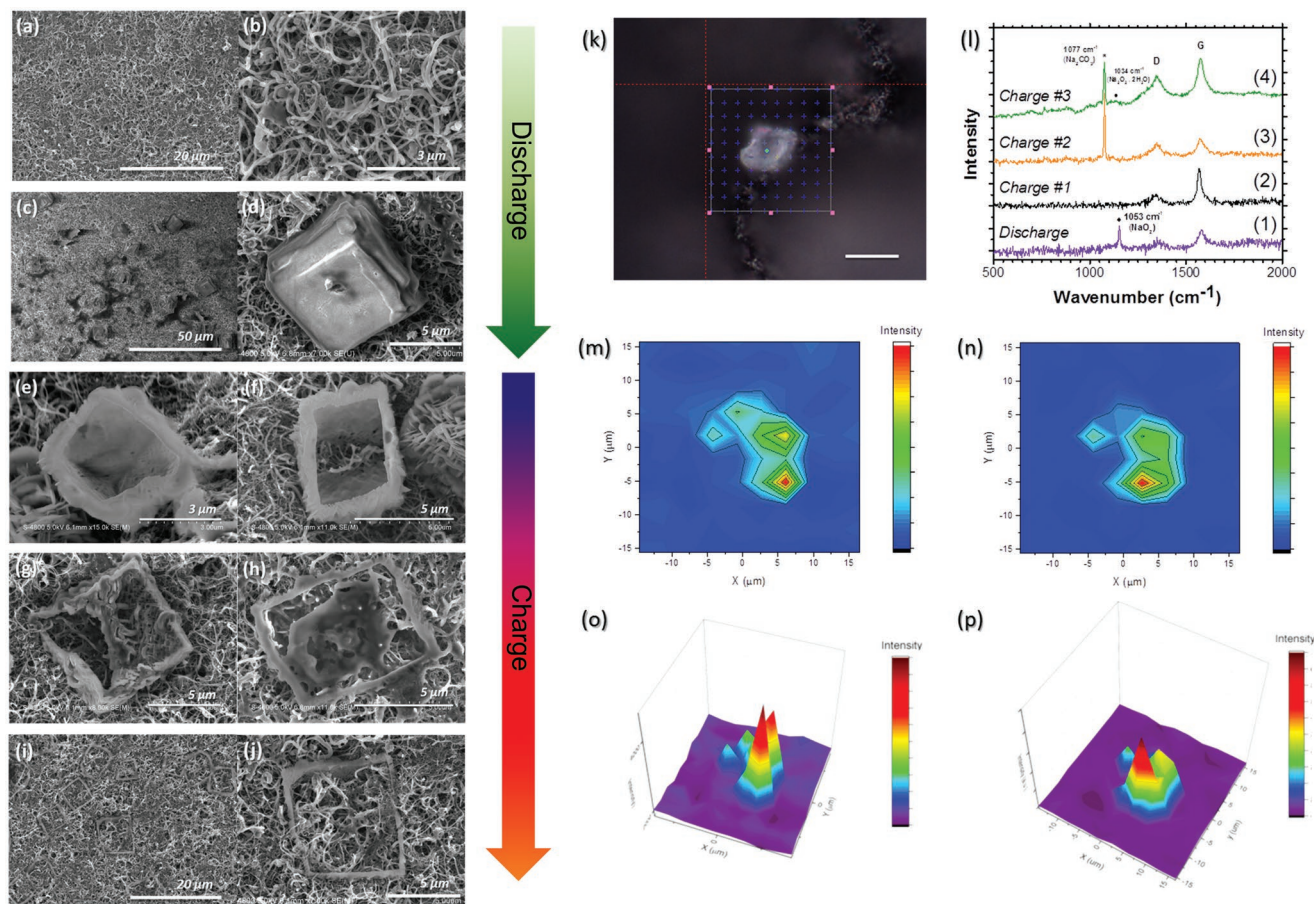
Figure 2. SEM picture of a,b) initial, c,d) fully discharged, e–h) partially, and i,j) fully charged CNT–PAN air electrodes; k) optical picture of the area for Raman mapping, the scale bar stands for 10 μm; the Raman spectra of 1) discharge and 2–4) different points of charge electrode; Raman mapping of region g) at m,o) 1080 cm^{-1} and n,p) 1036 cm^{-1}.

the side reaction between the NaO_2 cube with liquid electrolyte. Meanwhile, the chemical/electrochemical oxidation of carbon in the air electrode should have also contributed to the overall amount of Na_2CO_3 in the whole air electrode.

To verify the universality of this charging behavior of the cubic shape discharge product in Na–O_2 batteries, we also carried out the detailed SEM combined with energy-dispersive X-ray spectroscopy studies on the NCNT–PAN systems. Due to the straight nature of the NCNTs used in the present study compared to that of the tortuous CNTs, the stacking of NCNTs in the air electrode results in a more porous structure (**Figure 3**a,b). A tremendous amount of cube-shaped discharge product with smaller size aggregate along the NCNT units after a complete discharge (Figure 3c–j), which are more efficiently removed after recharging (Figure S4, Supporting Information). The reduced size of NaO_2 can be a result of altered local current density[28] and/or the higher absorption by NCNT than that of CNT.[24] The fact that less residual products are found in the recharged NCNT–PAN air electrode suggests an improved OER catalytic performance of NCNT over that of the pristine CNT electrode, contributing to their longer cycling lives. A survey on the partially charged NCNT–PAN air electrodes also reveals a similar evolution from solid cube to the combination of a shrunk core with robust outer box, hollow box, and frame

structure. Moreover, EDX mapping has been conducted on the products at different states of charge. The element mapping of Na, O, and C reveal an evolving trend during the cycling process (Figure 3k). In spite of the Na and O species that are distributed evenly over the products, the carbon content seems to readily increase at the outer box (Figure 3k–m), implying a difference between their chemical compositions. Moreover, the Na:O ratio of the core part of the partially charged electrode is also analyzed by EDX (Figure S5, Supporting Information).

Additionally, we observed an interesting phenomenon that the hollow/yolk–shell structure in the charged air electrode can be not obvious and needs to be revealed using an unconventional experimental condition for SEM. It can be sharply compared in Figure S6 (Supporting Information) that the SEM pictures using a regular low acceleration voltage of 5 kV does not depict the yolk–shell nature of the cubes, which is in contrast clearly observed in the pictures using 20 kV. Meanwhile in contrast, the cubes on the NCNT in fully discharged air electrode show a solid structure when observed at 20 kV (Figure S7, Supporting Information). This interest phenomenon may suggest that the thickness of the shell of the remaining semi charged products can only be penetrated by higher energy electrons and can be inspiring to other researchers who are interested in the discharge/charge products of Na–O_2 batteries.

**ADVANCED
SCIENCE NEWS**
www.advancedsciencenews.com

**ADVANCED
FUNCTIONAL
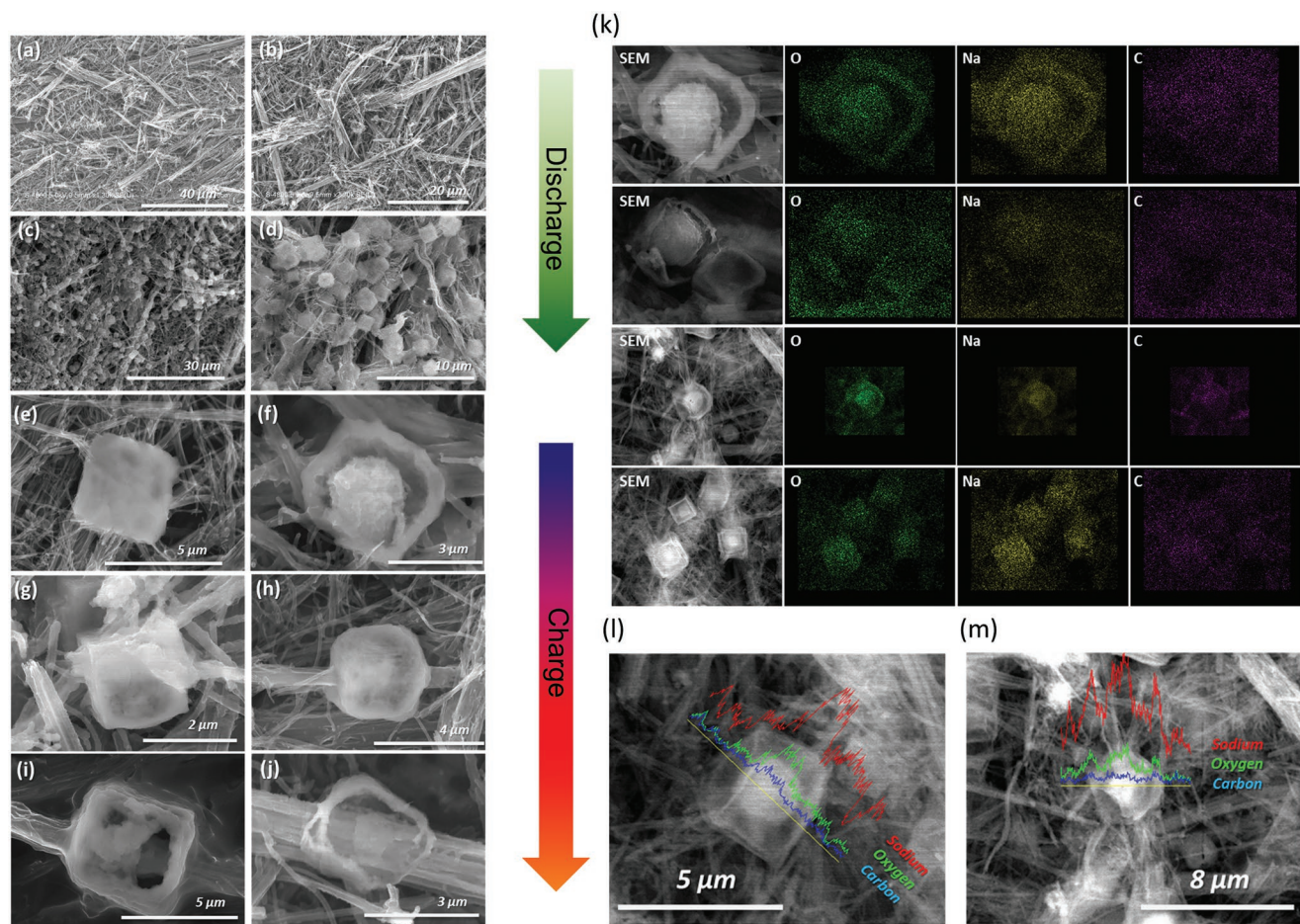MATERIALS**
www.afm-journal.de

Figure 3. SEM pictures of a,b) initial, c,d) discharged, and e–j) partially recharged NCNT–PAN air electrodes; k) EDX mapping and l,m) EDX line scanning of partially recharged NCNT–PAN air electrodes.

In order to further reveal the chemical compositions of the NCNT–PAN electrodes, soft X-ray absorption spectroscopy was utilized. The O K-edge XAS spectra were collected, which can resolve the features for a combination of the discharge products as well as the charging intermediate/side products in the electrode. Furthermore, the N K-edge was observed, which reflects the stability of N atoms in both NCNT and PAN. N K-edge XAS is conducted on the initial NCNT–PAN electrode as well as nitrogen gas N_2, pure NCNT, and PAN polymer powders for reference. The experimental setups and details are similar to our previous studies using XAS for Na–air batteries. As shown in our previous works, O K-edge XAS is highly effective in identifying the different oxygen-containing compounds in the cycled electrodes, such as superoxide, peroxide, and carbonates. The fluorescence yield (FLY) XAS spectra of the fully discharged (1.5 V), partially charged (to 3.5 V), and fully charged (to 4.5 V) electrodes (indicated in its charge and discharge curve shown in Figure S8 in the Supporting Information) display several distinct features (**Figure 4**-1). Three defined absorptions at 532.0, 532.9, and 534.4 eV can be observed, which can be assigned to NaO_2, Na_2O_2, and Na_2CO_3, respectively. The difference between the XAS spectra of NaO_2 and Na_2O_2 originates from the semi-occupied $\pi*$ antibonding orbital of NaO_2 and the fully occupied $\pi*$ antibonding orbital of NaO_2. Benefitting from this, the

analysis of the compositional changes of different oxygen containing species can be derived from the XAS spectra. Compared to the discharged electrode (Figure 4-1b,2b), the intensity of the XAS peak corresponding to Na_2O_2 significantly increased in the partially charged electrode to 3.5 V (Figure 4-1c,2c), but sharply weakened again when fully charged to 4.5 V (Figure 4-1d,2d). In contrast, the intensity of the XAS peak corresponding to Na_2CO_3 continuously increased during the charging process, while the XAS peak corresponding to NaO_2 kept diminishing during this process. These XAS results indicate the conversion of the NaO_2 discharge product to Na_2O_2 and Na_2CO_3. Meanwhile, a large amount of Na_2CO_3 remained undecomposed even after charging to 4.5 V (Figure S9, Supporting Information). These results are in good agreement with the above SEM and EDX results.

Moreover, we have investigated the N K-edge XAS of the initial, discharged, partially/fully charged electrodes, to reveal the stability of the active material, NCNT, and the binder, PAN. First, the N K-edge XAS of N_2, NCNT, and PAN standard samples are collected as references (Figure 4-3). The N K-edge XAS of N_2 primarily exhibit two groups of absorptions: the multi-peaks at 400.6, 400.9, 401.1, and 401.3 eV are attributed to the N 1s → $\pi*$ transitions,[29] and the broad peak at 405.6 eV, which is associated with the N 1s → $\sigma*$ transition.[29] On the other hand, the XAS of NCNT shows absorption peaks at several
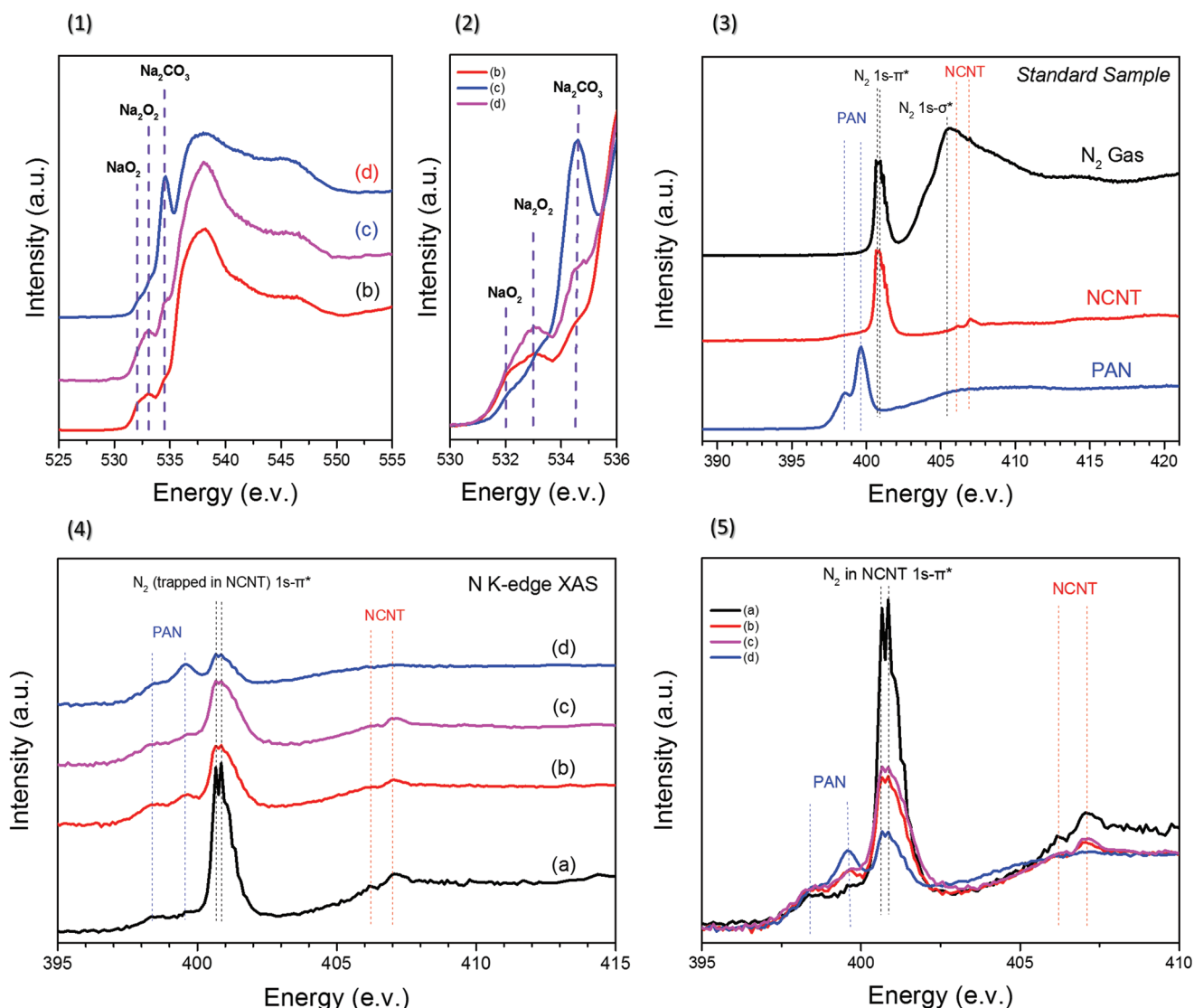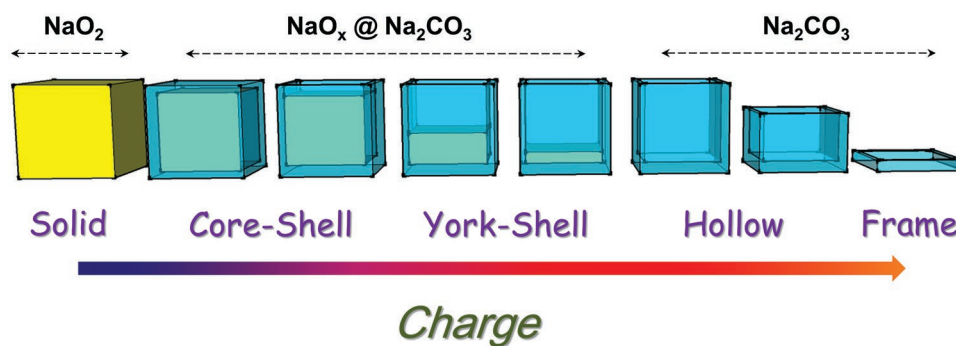
Figure 4. a,b) O K-edge and e,f) N K-edge XAS of NCNT–PAN air electrode at i) initial, ii) first discharged to 1.5 V, iii) first recharged to 3.5 V, and iv) first recharged to 4.5 V stages; the standard N K-edge XAS of N_2, NCNT, and PAN standard samples are shown in (c) for reference.

regions: the peaks at or close to 400.6 and 400.9 eV is consistent with N_2 gas,[29] which has been reported to be trapped in the inner space of NCNT;[30] meanwhile, the peaks at 406.0 and 406.9 eV should be related to the N atoms in NCNT shells.[30] These results are well consistent with previous reports. In contrast, the N K-edge XAS of PAN exhibits two sharp peaks at much lower energies of 398.5 and 399.6 eV, which should be attributed to the excitation of the N 1s electron to the unoccupied sp hybridization orbital of the $-C\equiv N$ functional group with triple bonds in the side chain of PAN.[31] Accordingly, it can be expected that these well-separated absorption peaks are able to provide in-depth insights on the states of NCNT and PAN in the electrode during discharge and charge processes. The N K-edge XAS of the initial NCNT–PAN simply shows the combination of the XAS of NCNT and PAN (Figure 4-4a,5a), implying their stable coexistence during electrode fabrication. Nonetheless, it can be observed that the XAS intensity of

N_2 trapped in NCNT as well as NCNT itself both significantly decreased during discharge (Figures 4-4b and 3-5b), while those corresponding to PAN only slightly change in terms of the peak intensity at 399.6 eV. After partial charging, no significant difference can be observed between the XAS of the electrodes charged to 3.5 V and the discharged state, implying minimal side reactions in this voltage range (Figures 4-4c and 3-5c). However, when fully charged, the XAS peaks of NCNT became totally undetectable, while the XAS peak of N_2 trapped in NCNT also sharply decayed (Figure 4-4d,5d). Meanwhile, the peak at 399.6 eV of PAN further increased while the other one at 398.4 eV remains unchanged. Thus, it may be inferred that the oxidation and destruction of NCNT is the major reason of the limited cycling performance of the battery. As a result, the side wall of the NCNT may have been broken due to the oxidation side reactions related to the superoxide during discharge and singlet oxygen species during charging, causing the releasing of trapped N_2 inside NCNT and

**ADVANCED
SCIENCE NEWS**
www.advancedsciencenews.com

**ADVANCED
FUNCTIONAL
MATERIALS**
www.afm-journal.de

Scheme 1. The morphological and chemically compositional evolution of cubic shape NaO_2 discharge products during recharging.

the diminished XAS intensity. In comparison, the structure and chemical state of PAN appear to be relatively stable during the cycling, except for that the increasing XAS peak which may imply the formation of hole in the partially occupied $-C\equiv N$ anti-bonding orbital. In contrast to the previously reported instability of PAN in a chemical environment, we infer that PAN is more likely to be a proton donor as the result of the effect of strong electron withdrawing $-C\equiv N$ functional groups on the main chain of PAN polymer. The different behavior of PAN against superoxide/peroxide in the practical battery here with the PAN polymer solution (or sol) dissolved in DMF against Li_2O_2 in the previous reference may be related to different possible reasons, including the different chemical/physical states as solid phase as the binder or being in solvating form in its DMF solution. Actually, there is a recent study showing that the dissolved PVDF in DMF can react with metallic lithium to produce LiF,[32] while the direct coating/contacting of PVDF onto Li foil does not show obvious reactions.[33] The difference between the reaction kinetics between the solid-state discharge product against the solid-state polymer binder and the solid-state peroxide against the liquid-state polymer solution/sol might be another reason. In addition, there is another possibility that the solubility of the formed reaction product between PAN and superoxide/peroxide in different solvents (ether in a practical Na–air battery and DMF for the PAN solution/sol) may also play an important role. It has been reported that the passive layer formed on polymer binder may prevent the further side reactions in a Li-air battery.[25a] Therefore, if such passive layer may be dissolved in or destroyed by certain types of solvent(s), it will lose the passive effect so that the continuous side reactions may occur as reported in previous references.[25b]

Combining evidences above the evidence shown above, it can be inferred that an interesting structure evolution of the discharge products during charging in Na–O$_2$ batteries have been discovered, including solid cube, core–shell, yolk–shell, hollow, and frame structure morphologies. The observed structures are related to the presence of different chemical components, which decompose electrochemically at different voltage ranges during the operation of these batteries. The overall schematic diagram is shown in **Scheme 1**.

The formation of the outer shell of the cube, which is determined to be mostly carbonates, should be related to at least two major factors. On one hand, it has been shown that ether electrolyte is only relatively stable against superoxides. Many recent studies show that sodium superoxide discharge products

in the cells readily react with ether electrolytes resulting in the consummation and conversion of NaO_2.[13,14,19,34] Moreover, the precipitation and dissolution of NaO_2 in ether electrolytes is also a reversible process. These observations are consistent with the formation of side products from the outer shell of the micrometer-sized NaO_2 cubes under kinetic control.

On the other hand, it has been also shown that an increased amount of carbonates had been detected during the charging process of Na–O$_2$ batteries. One possible explanation for this may be related to the formation of singlet oxygen during charging process, which has been recently emphasized in the studies of Li–O$_2$ and Na–O$_2$ batteries,[35] where singlet oxygen has been long known to be highly reactive and involved in many organic reactions. More research on the effects of this aspect may be also expected in future.

3. Conclusion

Herein, we provide a new understanding on the decomposition (charging) pathway of cubic shape NaO_2 as a discharge product of Na–O$_2$ batteries with CNT- and nitrogen-doped CNT-based air electrodes. Based on SEM, EDX mapping/line scanning, Raman spectra mapping, and synchrotron-based oxygen K-edge and nitrogen K-edge XAS results, a detailed electrochemical charging mechanism has been revealed during the charging process. A core–shell structure is found shortly after charging while the outer layer of the cubic shape intermediate is identified to be carbonate. The following charging process leads to the removal of the sodium peroxide-like phase core at a lower potential compared to the required voltage for the final removal of the Na_2CO_3 shell, resulting in yolk–shell, hollow, and frame structured interphases. Accordingly, we propose a core–shell model to elucidate the charging mechanism of Na–O$_2$ batteries and clarify the increasing overpotentials during this process, which are attributed to the formation of the interphases other than NaO_2. We believe that these new findings can provide more insight into the reaction route and mechanism of Na–O$_2$ batteries and contribute to their future developments.

Supporting Information

Supporting Information is available from the Wiley Online Library or from the author.

[1] a) J. Lu, L. Li, J. B. Park, Y. K. Sun, F. Wu, K. Amine, *Chem. Rev.* **2014**, *114*, 5611; b) A. C. Luntz, B. D. McCloskey, *Chem. Rev.* **2014**, *114*, 11721; c) F. Li, J. Chen, *Adv. Energy Mater.* **2017**, *7*, 1602934; d) Y. Liu, P. He, H. Zhou, *Adv. Energy Mater.* **2018**, *8*, 1701602; e) L. Ma, T. Yu, E. Tzoganakis, K. Amine, T. Wu, Z. Chen, J. Lu, *Adv. Energy Mater.* **2018**, *8*, 1800348; f) P. Zhang, Y. Zhao, X. Zhang, *Chem. Soc. Rev.* **2018**, *47*, 2921; g) Z. Zhao, J. Huang, Z. Peng, *Angew. Chem., Int. Ed.* **2018**, *57*, 3874.

[2] a) E. Peled, D. Golodnitsky, R. Hadar, H. Mazor, M. Goor, L. Burstein, *J. Power Sources* **2013**, *244*, 771; b) S. K. Das, S. Lau, L. A. Archer, *J. Mater. Chem. A* **2014**, *2*; c) S. Ha, J. K. Kim, A. Choi, Y. Kim, K. T. Lee, *ChemPhysChem* **2014**, *15*, 1971; d) P. Adelhelm, P. Hartmann, C. L. Bender, M. Busche, C. Eufinger, J. Janek, *Beilstein J. Nanotechnol.* **2015**, *6*, 1016; e) I. Landa-Medrano, C. Li, N. Ortiz-Vitoriano, I. Ruiz de Larramendi, J. Carrasco, T. Rojo, *J. Phys. Chem. Lett.* **2016**, *7*, 1161; f) H. Yadegari, Q. Sun, X. Sun, *Adv. Mater.* **2016**, *28*, 7065; g) K. Song, D. A. Agyeman, M. Park, J. Yang, Y. M. Kang, *Adv. Mater.* **2017**, *29*, 1606572; h) B. Sun, C. Pompe, S. Dongmo, J. Zhang, K. Kretschmer, D. Schröder, J. Janek, G. Wang, *Adv. Mater. Technol.* **2018**, *3*, 1800110.

[3] a) X. Ren, Y. Wu, *J. Am. Chem. Soc.* **2013**, *135*, 2923; b) X. Ren, M. He, N. Xiao, W. D. McCulloch, Y. Wu, *Adv. Energy Mater.* **2017**, *7*, 201601080; c) N. Xiao, R. T. Rooney, A. A. Gewirth, Y. Wu, *Angew. Chem., Int. Ed.* **2018**, *57*, 1227.

[4] Z. Lyu, Y. Zhou, W. Dai, X. Cui, M. Lai, L. Wang, F. Huo, W. Huang, Z. Hu, W. Chen, *Chem. Soc. Rev.* **2017**, *46*, 6046.

[5] J. Lu, Y. J. Lee, X. Luo, K. C. Lau, M. Asadi, H. H. Wang, S. Brombosz, J. Wen, D. Zhai, Z. Chen, D. J. Miller, Y. S. Jeong, J. B. Park, Z. Z. Fang, B. Kumar, A. Salehi-Khojin, Y. K. Sun, L. A. Curtiss, K. Amine, *Nature* **2016**, *529*, 377.

[6] C. Xia, R. Black, R. Fernandes, B. Adams, L. F. Nazar, *Nat. Chem.* **2015**, *7*, 496.

[7] Q. Sun, H. Yadegari, M. N. Banis, J. Liu, B. Xiao, X. Li, C. Langford, R. Li, X. Sun, *J. Phys. Chem. C* **2015**, *119*, 13433.

[8] L. Lutz, W. Yin, A. Grimaud, D. Alves Dalla Corte, M. Tang, L. Johnson, E. Azaceta, V. Sarou-Kanian, A. J. Naylor, S. Hamad, J. A. Anta, E. Salager, R. Tena-Zaera, P. G. Bruce, J. M. Tarascon, *J. Phys. Chem. C* **2016**, *120*, 20068.

[9] D. Schröder, C. L. Bender, M. Osenberg, A. Hilger, I. Manke, J. Janek, *Sci. Rep.* **2016**, *6*, 24288.

[10] B. Sun, K. Kretschmer, X. Xie, P. Munroe, Z. Peng, G. Wang, *Adv. Mater.* **2017**, *29*, 201606816.

[11] P. Hartmann, C. L. Bender, M. Vracar, A. K. Durr, A. Garsuch, J. Janek, P. Adelhelm, *Nat. Mater.* **2013**, *12*, 228.

[12] I. Landa-Medrano, A. Sorrentino, L. Stievano, I. Ruiz de Larramendi, E. Pereiro, L. Lezama, T. Rojo, D. Tonti, *Nano Energy* **2017**, *37*, 224.

[13] R. Black, A. Shyamsunder, P. Adeli, D. Kundu, G. K. Murphy, L. F. Nazar, *ChemSusChem* **2016**, *9*, 1795.

[14] a) M. N. Banis, H. Yadegari, Q. Sun, T. Regier, T. Boyko, J. Zhou, Y. M. Yiu, R. Li, Y. Hu, T. K. Sham, X. Sun, *Energy Environ. Sci.* **2018**, *11*, 2073; b) H. Yadegari, M. Norouzi Banis, X. Lin, A. Koo, R. Li, X. Sun, *Chem. Mater.* **2018**, *30*, 5156.

[15] W.-J. Kwak, L. Luo, H.-G. Jung, C. Wang, Y.-K. Sun, *ACS Energy Lett.* **2018**, *3*, 393.

[16] L. Lutz, W. Dachraoui, A. Demortière, L. R. Johnson, P. G. Bruce, A. Grimaud, J.-M. Tarascon, *Nano Lett.* **2018**, *18*, 1280.

[17] Q. Liu, T. Yang, C. Du, Y. Tang, Y. Sun, P. Jia, J. Chen, H. Ye, T. Shen, Q. Peng, L. Zhang, J. Huang, *Nano Lett.* **2018**, *18*, 3723.

[18] Q. Sun, J. Liu, X. Li, B. Wang, H. Yadegari, A. Lushington, M. N. Banis, Y. Zhao, W. Xiao, N. Chen, J. Wang, T.-K. Sham, X. Sun, *Adv. Funct. Mater.* **2017**, *27*, 1606662.

[19] J. Kim, H. Park, B. Lee, W. M. Seong, H. D. Lim, Y. Bae, H. Kim, W. K. Kim, K. H. Ryu, K. Kang, *Nat. Commun.* **2016**, *7*, 10670.

[20] a) X. Lin, Q. Sun, H. Yadegari, X. Yang, Y. Zhao, C. Wang, J. Liang, A. Koo, R. Li, X. Sun, *Adv. Funct. Mater.* **2018**, *28*, 1801904; b) B. Sun, P. Li, J. Zhang, D. Wang, P. Munroe, C. Wang, P. H. L. Notten, G. Wang, *Adv. Mater.* **2018**, *30*, 201801334.

[21] Q. Sun, X. Lin, H. Yadegari, W. Xiao, Y. Zhao, K. R. Adair, R. Li, X. Sun, *J. Mater. Chem. A* **2018**, *6*, 1473.

[22] R. Black, S. H. Oh, J. H. Lee, T. Yim, B. Adams, L. F. Nazar, *J. Am. Chem. Soc.* **2012**, *134*, 2902.

[23] Z. E. Reeve, C. J. Franko, K. J. Harris, H. Yadegari, X. Sun, G. R. Goward, *J. Am. Chem. Soc.* **2017**, *139*, 595.

[24] Q. Sun, H. Yadegari, M. N. Banis, J. Liu, B. Xiao, B. Wang, S. Lawes, X. Li, R. Li, X. Sun, *Nano Energy* **2015**, *12*, 698.

[25] a) E. Nasybulin, W. Xu, M. H. Engelhard, Z. Nie, X. S. Li, J.-G. Zhang, *J. Power Sources* **2013**, *243*, 899; b) C. V. Amanchukwu, J. R. Harding, Y. Shao-Horn, P. T. Hammond, *Chem. Mater.* **2015**, *27*, 550.

[26] Q. Sun, Y. Yang, Z.-W. Fu, *Electrochem. Commun.* **2012**, *16*, 22.

[27] C. Xia, R. Fernandes, F. H. Cho, N. Sudhakar, B. Buonacorsi, S. Walker, M. Xu, J. Baugh, L. F. Nazar, *J. Am. Chem. Soc.* **2016**, *138*, 11219.

[28] N. Ortiz-Vitoriano, T. P. Batcho, D. G. Kwabi, B. Han, N. Pour, K. P. Yao, C. V. Thompson, Y. Shao-Horn, *J. Phys. Chem. Lett.* **2015**, *6*, 2636.

[29] a) S. Fatehi, C. P. Schwartz, R. J. Saykally, D. Prendergast, *J. Chem. Phys.* **2010**, *132*, 094302; b) A. V. Okotrub, M. A. Kanygin, L. G. Bulusheva, D. V. Vyalikh, *Fullerenes, Nanotubes, Carbon Nanostruct.* **2010**, *18*, 551.

[30] J. Zhou, J. Wang, H. Liu, M. N. Banis, X. Sun, T.-K. Sham, *J. Phys. Chem. Lett.* **2010**, *1*, 1709.

[31] a) S. Carniato, R. Taieb, E. Kukk, Y. Luo, B. Brena, *J. Chem. Phys.* **2005**, *123*, 214301; b) P. Leinweber, J. Kruse, F. L. Walley, A. Gillespie, K. U. Eckhardt, R. I. Blyth, T. Regier, *J. Synchrotron Radiat.* **2007**, *14*, 500.

[32] J. Lang, Y. Long, J. Qu, X. Luo, H. Wei, K. Huang, H. Zhang, L. Qi, Q. Zhang, Z. Li, H. Wu, *Energy Storage Mater.* **2019**, *16*, 85.

[33] J. Luo, C.-C. Fang, N.-L. Wu, *Adv. Energy Mater.* **2018**, *8*, 1701482.

[34] T. Liu, G. Kim, M. T. Casford, C. P. Grey, *J. Phys. Chem. Lett.* **2016**, *7*, 4841.

[35] L. Schafzahl, N. Mahne, B. Schafzahl, M. Wilkening, C. Slugovc, S. M. Borisov, S. A. Freunberger, *Angew. Chem., Int. Ed.* **2017**, *56*, 15728.